

Xanthohumol attenuates renal ischemia/reperfusion injury by inhibiting ferroptosis

ZHE TANG¹, YE FENG¹, WEN NIE² and CHENGLONG LI³

¹Department of Urology, The First People's Hospital of Jing Zhou, The First Affiliated Hospital of Yangtze University, Jingzhou, Hubei 434000; ²Department of Training Injury Prevention and Treatment, Wuhan Armed Police Special Service Rehabilitation Center, Wuhan, Hubei 430074; ³Department of Urology, Renmin Hospital of Wuhan University, Wuhan, Hubei 430060, P.R. China

Received June 30, 2023; Accepted August 22, 2023

DOI: 10.3892/etm.2023.12269

Abstract. Ischemia/reperfusion injury (IRI) is a notable contributor to kidney injury, but effective prevention and treatment options are limited. The present study aimed to evaluate the impact of xanthohumol (XN), a kind of flavonoid, on renal IRI and its pathological process in rats. Rats and HK-2 cells were divided into five groups: Sham (control), IR [hypoxia-reoxygenation (HR)], IR (HR) + XN, IR (HR) + erastin or IR (HR) + XN + erastin. The effects of XN and erastin (a ferroptosis inducer) on IRI in rats were evaluated using blood urea nitrogen, plasma creatinine, glutathione, superoxide dismutase and malondialdehyde kits, western blotting, cell viability assay, hematoxylin and eosin staining and reactive oxygen species (ROS) detection. Nrf2 small interfering (si)RNA was used to investigate the role of the Nrf2/heme oxygenase (HO)-1 axis in XN-mediated protection against HR injury. Cell viability, ROS levels and expression of ferroptosis-related proteins were analyzed. Following IR, renal function of rats was severely impaired and oxidative stress and ferroptosis levels significantly increased. However, XN treatment decreased renal injury and inhibited oxidative stress and ferroptosis in renal tubular epithelial cells. Additionally, XN upregulated the Nrf2/HO-1 signaling pathway and Nrf2-siRNA reversed the renoprotective effect of XN. XN effectively decreased renal IRI by inhibiting ferroptosis and oxidative stress and its protective mechanism may be associated with the Nrf2/HO-1 signaling pathway.

Introduction

Acute kidney injury (AKI) is a common clinical syndrome characterized by rapid-onset kidney function damage, which leads to chronic and end-stage kidney disease (1). Renal ischemia/reperfusion injury (RIRI) is the primary pathogenic mechanism underlying AKI in which the renal blood supply is constrained and then restored (2). Reactive oxygen species (ROS) overproduction, neutrophil-endothelial cell adhesion and alterations to the microenvironment are the primary pathological mechanisms of RIRI (3,4). Oxidative stress and ferroptosis play crucial roles in RIRI (5-8).

Ferroptosis is a type of cell death that occurs due to iron-dependent lipid peroxidation (9). Ferroptosis was first proposed by Dixon *et al* (10) to describe a form of programmed cell death dependent on cellular iron ions that occurs after treatment with the small molecule compound erastin. Erastin inhibits cystine uptake that leads to depletion of reduced glutathione (GSH), hindering the antioxidant capacity of glutathione peroxidase 4 (GPX4), causing an imbalance of intracellular redox levels and inability to eliminate lipid peroxidation products (10). Tuo *et al* (5) showed that ferroptosis inhibitors ferrostatin-1 and liproxstatin-1 notably decrease the infarction volume caused by cerebral IRI in rats by limiting lipid peroxidation and inhibiting ferroptosis. In addition, a previous study confirmed the role of ferroptosis in the pathogenesis of IRI-mediated kidney injury (11). Tao *et al* (12) confirmed that decreased lipid peroxidation and ferroptosis inhibition can reduce RIRI.

Various fruits, vegetables and plant-based foods such as quercetin, citrus, soy and tea contain flavonoids, compounds that exhibit renal-protective effects by chelating redox-active metals, which inhibit lipid peroxidation (13). Xanthohumol (XN), the primary active ingredient in hops, is a flavonoid with various biological properties, including antioxidation, antitumor and antibacterial properties (14,15). Previous studies have shown that XN promotes neuronal differentiation and neurite growth and serves a neuroprotective role against ischemic stroke in rats (16,17). To the best of our knowledge, however, the renal protective effect of XN has not been reported. The present study aimed to investigate whether XN alleviates IR-induced ferroptosis and its underlying mechanisms.

Correspondence to: Dr Chenglong Li, Department of Urology, Renmin Hospital of Wuhan University, 238 Jiefang Road, Wuhan, Hubei 430060, P.R. China
E-mail: lichenglong2010@tutaimail.com

Key words: xanthohumol, renal ischemia/reperfusion injury, ferroptosis, oxidative stress

Materials and methods

Chemicals. XN was purchased from Shanghai Macklin Biochemical Co., Ltd. (cat. no. 6754-58-1). Erastin was purchased from MedChemExpress (cat. no. HY-15763).

Animals. A total of 30 male Sprague-Dawley rats (age, 6 weeks old; weight, 200-220 g) were obtained from the Animal Center of Wuhan University, Wuhan, China. The rats were maintained with standard feeding conditions including food and water *ad libitum*, a 12 h light/dark cycle, 20-25°C and 50-65% humidity.

RIRI model. Rats were fasted for 8 h before surgery. All rats were randomly divided into five groups (six rats per group): Sham, IR, IR + XN, IR + erastin or IR + XN + erastin groups. To explore the effect of XN on RIRI, XN group rats were intraperitoneally injected with 0.4 mg/kg XN (16) 10 min before IR. The erastin group rats were intraperitoneally injected with 10 mg/kg erastin (18) 10 min before IR. A total of 50 mg/kg pentobarbital sodium was injected intraperitoneally to induce anesthesia before surgery. The limbs of the rats were fixed and the surgical skin area was disinfected. The renal pedicle was exposed via abdominal incision, and bilateral renal arteries were clamped for 45 min. The hemostatic forceps were loosened during reperfusion and the color change of the kidney was observed. After blood flow returned to normal, the incision was sutured. The sham group only underwent abdominal incision without clamping the renal pedicle. After 24 h, rats were humanely euthanized under anesthesia by intraperitoneal injection with 1% pentobarbital sodium (150 mg/kg). Rat kidneys were harvested and serum samples were collected.

Cell culture. HK-2 cells, a human renal tubular epithelial cell line, were obtained from the National Collection of Authenticated Cell Cultures (Beijing, China). HK-2 cells were cultured in DMEM (cat. no. 12430112) with 1% penicillin-streptomycin solution (cat. no. 15140122) and 10% fetal bovine serum (cat. no. 16140089; all Gibco; Thermo Fisher Scientific, Inc.). Cells were cultured in a 37°C incubator with 5% CO₂. All cells were randomly divided into five groups: Control, IR, IR + XN, IR + erastin or IR + XN + erastin.

Hypoxia-reoxygenation (HR) model. Following starvation in serum-free DMEM for 12 h at 37°C, HK-2 cells were transferred to a 37°C tri-gas incubator containing 95% N₂ to induce hypoxia for 8 h.

Treatment protocols in vitro. To investigate the effect of ferroptosis and XN, HK-2 cells were incubated with 10 μM XN (19) or erastin (20) at the beginning of reoxygenation. HK-2 cells were transfected with either control small interfering RNA (si-con; GenePharma Co., Ltd.) or Nrf2 siRNA (si-Nrf2; GenePharma Co., Ltd.) for 48 h before IR to evaluate the effect of Nrf2. The HK-2 cells were transfected with si-Nrf2 (5'-GCA CCUUAUAUCUCGAAGUTT-3') or non-targeting scrambled (used as si-con) oligonucleotides (5'-UUCUCCGAACGUGUC ACGUTT-3') using Lipofectamine® 2000 (Invitrogen; Thermo Fisher Scientific, Inc.) according to the instructions provided

by the manufacturer. The cells were subjected to treatment 24 h after transfection.

Cell viability assay. Cell viability assay was performed using Cell Counting Kit-8 (CCK-8; cat. no. C0038; Beyotime Institute of Biotechnology). HK-2 cells were transferred into 96-well plates at a density of 1x10⁴ cells/well and cultured for 12 h in a 37°C thermostatic incubator. Following treatment with either XN or erastin for 4 h, 10 μl CCK-8 solution was added to the 96-well plates and cells were incubated for 1 h. A microplate reader (PerkinElmer, Inc.) was used to measure absorbance at 450 nm.

Renal function and histopathological analysis. Renal function was measured using serum creatinine (Scr) and blood urea nitrogen (BUN). Serum was separated by centrifugation at 3,000 x g and at 4°C, and Scr and BUN levels were determined by staff at the Clinical Laboratory of Renmin Hospital of Wuhan University, who were blinded to the treatments given. Blood samples were stored at -80°C for analysis. Rat kidney samples were collected and fixed in 4% formaldehyde for 24 h at room temperature, dehydrated with 95% ethanol and embedded in 55°C paraffin, and then cut into 4-μm sections. The sections were stained with hematoxylin and eosin (H&E) to assess the histopathological changes. The slides were stained with hematoxylin, and incubated at room temperature for 4 min. The slides were incubated in water at 25°C for 30 min. The slides were dehydrated in 100% ethanol for 10 min three times, and were stained with eosin at room temperature for 4 min. The slides were dehydrated in 100% ethanol for 10 min three times, and mounted under cover slips. The slides were observed under x200 magnification using a light microscope (Olympus Corporation). A total of five different fields of view were observed. The severity of RIRI was assessed according to Paller's score (21). The histopathological changes of kidney tissue were analyzed and graded as follows: 0, no damage; 1, mild damage, including rounded epithelial cells and dilated tubular lumen; 2, moderate damage, including substantially dilated lumen, flattened epithelial cells and nuclear staining loss; and 3, severe damage, including destroyed tubules with no nuclear staining of epithelial cells. The evaluation of histological data was performed by two independent observers, blinded to the experimental group.

Reverse transcription-quantitative PCR (RT-qPCR). Total RNA was extracted using TRIzol® reagent (Vazyme Biotech Co., Ltd.) in accordance with the manufacturer's instructions. After quantification with a Nanodrop spectrophotometer (Thermo Fisher Scientific, Inc.), 1 μg RNA sample was reverse transcribed into cDNA (42°C, 2 min; 37°C, 15 min; 85°C, 5 sec) using a First Strand cDNA Synthesis kit (Thermo Fisher Scientific, Inc.). Subsequently, the RT-qPCR assay was performed based on the descriptions of a SYBR Premix Ex Taq II kit (Vazyme Biotech Co., Ltd.) in an ABI PRISM 7700 Sequence Detection System (Applied Biosystems; Thermo Fisher Scientific, Inc.). GAPDH was used as the internal reference to normalize mRNA expression levels. The calculation of mRNA levels was executed using the 2^{-ΔΔC_q} method (22). The qPCR thermocycling conditions were as follows: Initial denaturation at 95°C for 30 sec, followed by annealing and

Table I. Sequences of primer pairs for quantitative PCR.

Primer	Forward (5'-3')	Reverse (5'-3')
Nrf2	CCCAGCACATCCAGACAGAC	TATCCAGGGCAAGCGACTC
Heme oxygenase-1	CCCTTCCTGTGTCTTCCTTTG	ACAGCCGCCTCTACCGACCACA
GAPDH	GACATGCCGCTGGAGAAAC	AGCCAGGATGCCCTTTAGT

elongation for 39 cycles of 95°C for 15 sec, 60°C for 30 sec and 72°C for 30 sec, and a final extension at 72°C for 2 min. The primer sequences used in the present study are shown in Table I.

Western blotting. The cells or tissues were lysed in ice-cold modified RIPA lysis buffer (50 mM Tris-HCl, pH 7.5, 150 mM NaCl, 50 mM NaF, 0.5% deoxycholic acid, 1% NP-40, 1 mM sodium orthovanadate and 0.1% SDS). The insoluble material was then removed by centrifugation at 12,000 x g for 15 min at 4°C. The protein concentration of each sample was measured using a BCA kit (cat. no. A045-4-2; Nanjing Jiancheng Bioengineering Institution). Total protein (10 µg/lane) was separated using SDS-PAGE (10% gels) and transferred to a PVDF membrane. Membranes were incubated with primary antibodies against GPX4 (1:1,000; cat. no. 67763-1-Ig; Proteintech Group, Inc.), long-chain acyl-CoA synthetase (ACSL4; 1:1,000; cat. no. 22401-1-AP; Proteintech Group, Inc.), Nrf2 (1:1,000; cat. no. 80593-1-RR; Proteintech Group, Inc.), heme oxygenase (HO)-1 (1:1,000; cat. no. 10701-1-AP; Proteintech Group, Inc.) or GAPDH (1:1,000; cat. no. 60004-1-Ig; Proteintech Group, Inc.) overnight at 4°C following blocking with 5% BSA for 2 h at room temperature (Beijing Solarbio Science & Technology Co., Ltd.). Then, membranes were washed in TBS containing 0.1% Tween-20 and incubated for 2 h at room temperature with corresponding secondary antibodies. The secondary antibodies used were HRP-conjugated anti-rabbit (1:1,000; cat. no. sc-2370) and anti-mouse (1:1,000; cat. no. sc-516102) (Santa Cruz Biotechnology, Inc.) were used. The membranes were visualized using an ECL kit (cat. no. W028-2-1; Nanjing Jiancheng Bioengineering Institution) and band intensities were quantified using ImageJ (version 1.8.0; National Institutes of Health).

Detection of oxidative stress indicators. The kidney tissues or HK-2 cells were homogenized and centrifuged at 4°C for 10 min at 10,000 x g. Then, the activities of superoxide dismutase (SOD), malondialdehyde (MDA) and GSH were determined using commercial kits (cat. nos. S0131S, S0101S and S0053, respectively; Beyotime Institute of Biotechnology) based on the manufacturer's protocols and the OD values were determined at 560 (SOD), 412 (GSH), 532 and 600 (MDA) nm, respectively, using a microplate reader.

ROS levels in kidney tissues. Dihydroethidium (DHE) fluorescence probe (cat. no. D7008; Sigma-Aldrich; Merck KGaA) was used to evaluate the level of ROS in the kidney tissues. Kidney tissues were placed in optimal cutting temperature embedding medium (Servicebio, Inc.), frozen for 3 min at -20°C and cut into 30 µm-thick sections by a freezing microtome.

The DHE probe was dissolved in dimethyl sulfoxide and then diluted with phosphate-buffered saline to a working solution of 10 µmol/l. DHE probe working solution (100 µl) was added onto the surface of the section, which was then promptly placed in a light-tight wet box for 30 min at 37°C, in order to oxidize DHE and generate ethidium bromide (EB). The EB binds to DNA in the cell nucleus to produce red fluorescence under UV light. Subsequently, unreacted probes were washed away and the sample was observed under a fluorescence microscope. Under excitation at a wavelength of 490 nm and an emission wavelength of 520 nm, the signal intensity of the red fluorescence was observed. Microscopic imaging analysis was adopted for image acquisition. Image-Pro Plus 6.0 (Media Cybernetics, Inc.) was used for the quantitative analysis of the fluorescence intensity of the image.

ROS levels of HK-2 cells. Intracellular ROS production was assessed using a fluorescent probe, DCFH-DA, using flow cytometric analysis, as previously described (23). Detection of ROS was based on the fact that intracellular ROS are able to oxidize DCFH, yielding the fluorescent product, 2',7'-dichlorofluorescein (DCF). Following an incubation of the cells with 0, 15, or 30 mM formate at 37°C for 24 h, the supernatant was removed (300 x g at room temperature for 10 min), and the cells were washed with PBS three times. The cells were subsequently harvested and suspended in PBS. DCFH-DA (10 µM final concentration) probe (cat. no. D6883; Sigma-Aldrich; Merck KGaA) was added and the mixture was incubated at 37°C for 15 min. Finally, ROS generation was measured, according to the fluorescence intensity (FL-1; 530 nm) of 10⁴ cells using a flow cytometer (FACSCalibur; BD Biosciences).

Statistical analysis. GraphPad (version 8.0.1; Dotmatics) was used to analyze experimental data. Data are presented as mean ± the standard deviation from three independent experiments. The comparisons between multiple groups were conducted by one-way ANOVA followed by Tukey's post hoc test. P<0.05 was considered to indicate a statistically significant difference.

Results

XN significantly decreases RIRI. In the sham group, the renal tubular lumen was not dilated, glomerular structure was intact, and the renal tubular epithelial cells were healthy. However, in the IR group, there was a noticeable glomerular lesion, renal tubular epithelial cells were flat, the renal tubular lumen was occluded and there were instances of bleeding and cell abscission. These changes indicated diffuse damage. By contrast, the XN + IR group showed decreased glomerular damage,

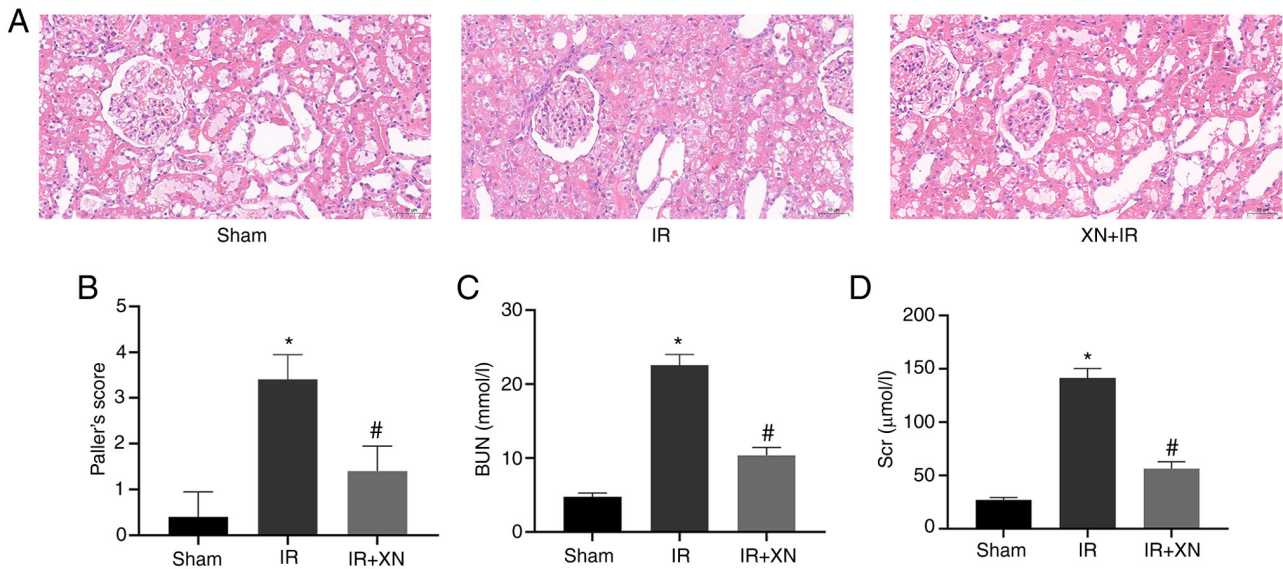


Figure 1. XN attenuates IR-induced kidney injury. Rats underwent sham operation or RIRI with or without XN. (A) Representative images of hematoxylin and eosin staining in kidney sections; magnification, x400. (B) Paller's score of kidney injury. Concentrations of (C) BUN and (D) SCr in rats. * $P < 0.05$ vs. sham; # $P < 0.05$ vs. IR. XN, xanthohumol; RIRI, renal ischemia/reperfusion injury; BUN, blood urea nitrogen; SCr, serum creatinine.

although the renal tubular lumen was still partially occluded and the morphology of renal tubular epithelial cells was flattened with loss of the brush border (Fig. 1A and B).

The concentrations of BUN and SCr in the IR group were significantly higher than those in the sham group, while levels of BUN and SCr in the XN + IR group were lower than those in the IR group (Fig. 1C and D).

XN attenuates ferroptosis during RIRI. To determine whether the protection against RIRI by XN is related to ferroptosis, the production of ROS and the levels of SOD, MDA and GSH were measured. IR significantly increased ROS and MDA levels and decreased the activity of SOD and GSH, while XN inhibited IR-induced oxidative damage (Fig. 2A-E). The expression of the ferroptosis-related proteins GPX4 and ACSL4 was determined. The expression of the pro-ferroptosis protein ACSL4 increased in the IR group, while expression of the anti-ferroptosis protein GPX4 decreased in the IR group. However, XN partially reversed these changes and erastin blocked the inhibitory effect of XN on ferroptosis (Fig. 2F-H). In general, XN attenuated ferroptosis during RIRI.

XN inhibits HR-induced damage and ferroptosis in HK-2 cells. An HR model of the renal tubular epithelial cell line HK-2 was established to determine whether XN prevents HR-induced damage and ferroptosis. The CCK-8 assay was performed to evaluate cell viability. HR decreased cell viability and XN prevented cell death caused by HR. However, erastin reversed the protective effect of XN on HK-2 cells (Fig. 3A). In addition, HR increased and decreased the levels of MDA and SOD, respectively, in HK-2 cells. XN increased SOD and GSH and decreased MDA in HK-2 cells. Erastin reversed the inhibitory effect of XN on ROS levels in HK-2 cells (Fig. 3B-D). Similarly, XN inhibited the increase of ACSL4 expression induced by HR, enhanced activity of GSH and upregulated

the expression of GPX4, while erastin blocked the inhibitory effect of XN on ferroptosis (Fig. 3E-G).

XN upregulates the Nrf2/HO-1 signaling pathway. RT-qPCR showed that XN significantly upregulated mRNA levels of Nrf2 and HO-1 in IR+XN group (Fig. 4A and B). Western blotting showed that IR upregulated the expression of nuclear Nrf2 and cytoplasmic HO-1 in renal tissue, while XN further upregulated expression of Nrf2 and HO-1 (Fig. 4C-E). Similar results were obtained in the HR model of cells (Fig. 4F-H).

XN inhibits IR-induced ferroptosis via the Nrf2/HO-1 signaling pathway. To explore the role of the Nrf2/HO-1 axis in XN-mediated protection against IRI, si-Nrf2 was used to knock down Nrf2. Nrf2 expression was significantly decreased following si-Nrf2 transfection (Fig. 5A and B). XN prevented oxidative damage (XN upregulated the levels of SOD and GSH levels, and downregulated the MDA level) and decreased cell viability caused by HR, while si-Nrf2 transfection eliminated this inhibitory effect (Fig. 5C-F). Consistently, si-Nrf2 transfection inhibited the effect of XN on HR-induced upregulation and downregulation of GPX4 and ACSL4 expression, respectively (Fig. 5G-K). DCFH-DA fluorescent probe assessed intracellular ROS levels in HK-2 cells following HR. The results showed that XN decreased ROS levels, while si-Nrf2 transfection increased ROS levels (Fig. 5L and M).

Discussion

AKI is a prevalent clinical syndrome characterized by rapid loss of renal function (24). AKI primarily manifests as a reduction in glomerular filtration rate and renal excretion dysfunction, coupled with a rapid increase in BUN and SCr or hypouricemia (24,25). Although the pathogenesis of AKI is complex, RIRI is a common cause of AKI and it is

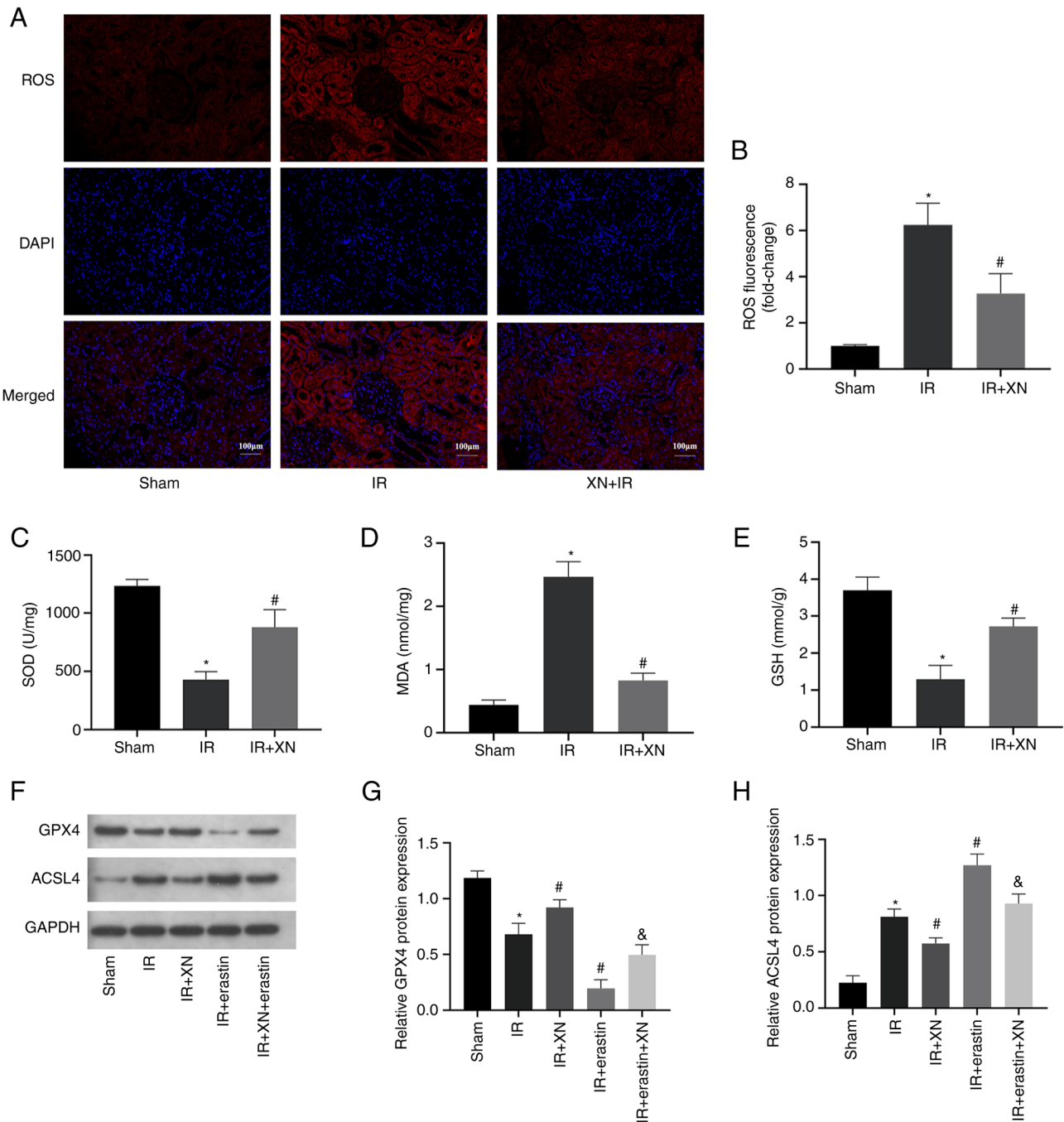


Figure 2. XN prevents ferroptosis during RIRI. (A) ROS production in kidney tissue was measured by the dihydroethidium fluorescence probe; magnification, $\times 200$. (B) Quantitative analysis of ROS levels. (C) SOD, (D) MDA and (E) GSH levels in kidney tissues of rats. (F) Western blotting of (G) GPX4 and (H) ACSL4 in kidney tissues. * $P < 0.05$ vs. sham, # $P < 0.05$ vs. IR and & $P < 0.05$ vs. XN + IR. XN, xanthohumol; RIRI, renal ischemia/reperfusion injury; ROS, reactive oxygen species; SOD, superoxide dismutase; MDA, malondialdehyde; GSH, glutathione; ACSL4, long-chain acyl-CoA synthetase.

prevalent in critically ill patients and those undergoing major surgery (26,27). Additionally, renal insufficiency, such as that occurring during cardiac surgery using a cardiopulmonary bypass machine, is a leading cause of severe AKI (27).

RIRI is a complex pathophysiological process that results in a decline in kidney function, leading to damage and life-threatening consequences. Currently, there is a lack of effective RIRI-specific drugs, and ongoing research aims to develop potential treatments (28). Natural products, such as traditional Chinese medicine, have gained attention due to their low toxicity and high biological activity (29,30).

XN is a primary active ingredient in hops and belongs to the isoprene flavonoid compound class (31). XN has various biological functions, such as anti-tumor and anti-inflammatory effects and regulation of lipid metabolism (32-37). XN induces the apoptosis of activated hepatic stellate cells *in vitro* in a dose-dependent manner and decreases expression of some pro-inflammatory response factors, such as monocyte chemoattractant protein-1 in hepatic stellate cells (38). In addition, XN has a notable anticancer effect and inhibits the growth of tumor blood vessels by blocking the endothelial nuclear factor NF- κ B and Akt signaling pathways (39). XN also inhibits production

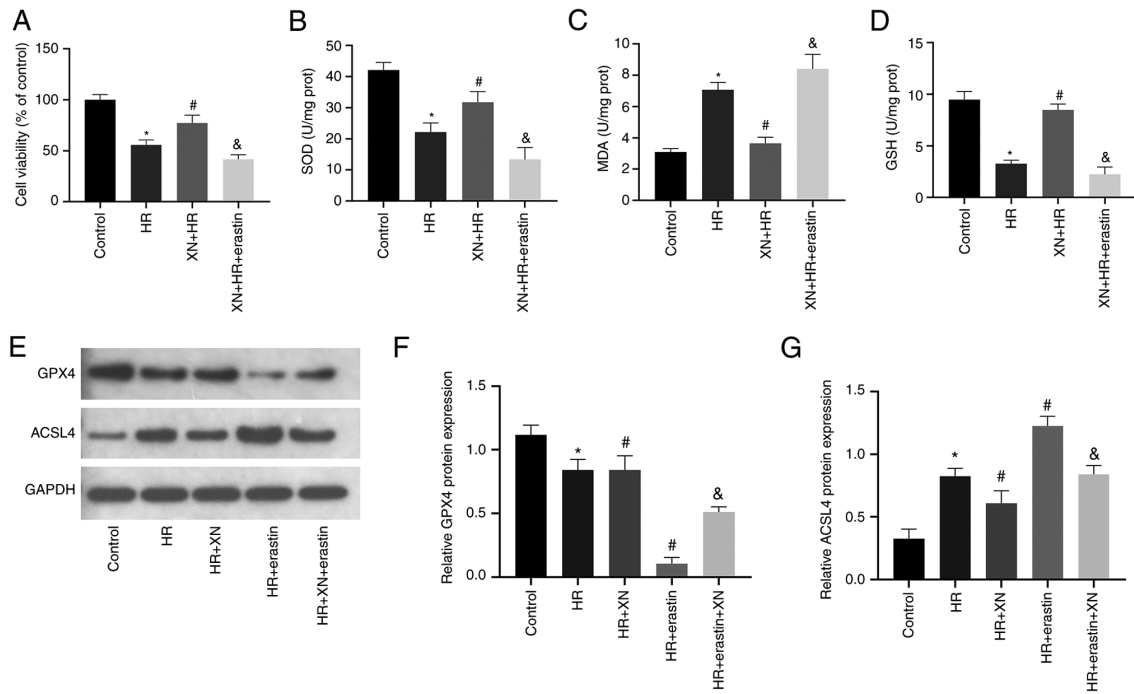


Figure 3. XN inhibits HR-induced ferroptosis in HK-2 cells. (A) Cell Counting Kit-8 was used to evaluate cell viability. (B) SOD, (C) MDA and (D) GSH levels in HK-2 cells. (E) Western blotting of (F) GPX4 and (G) ACSL4 in HK-2 cells. * $P < 0.05$ vs. control, # $P < 0.05$ vs. HR and & $P < 0.05$ vs. XN + HR. XN, xanthohumol; HR, hypoxia-reoxygenation; SOD, superoxide dismutase; MDA, malondialdehyde; GSH, glutathione; prot, protein; GPX4, glutathione peroxidase 4; ACSL4, long-chain acyl-CoA synthetase.

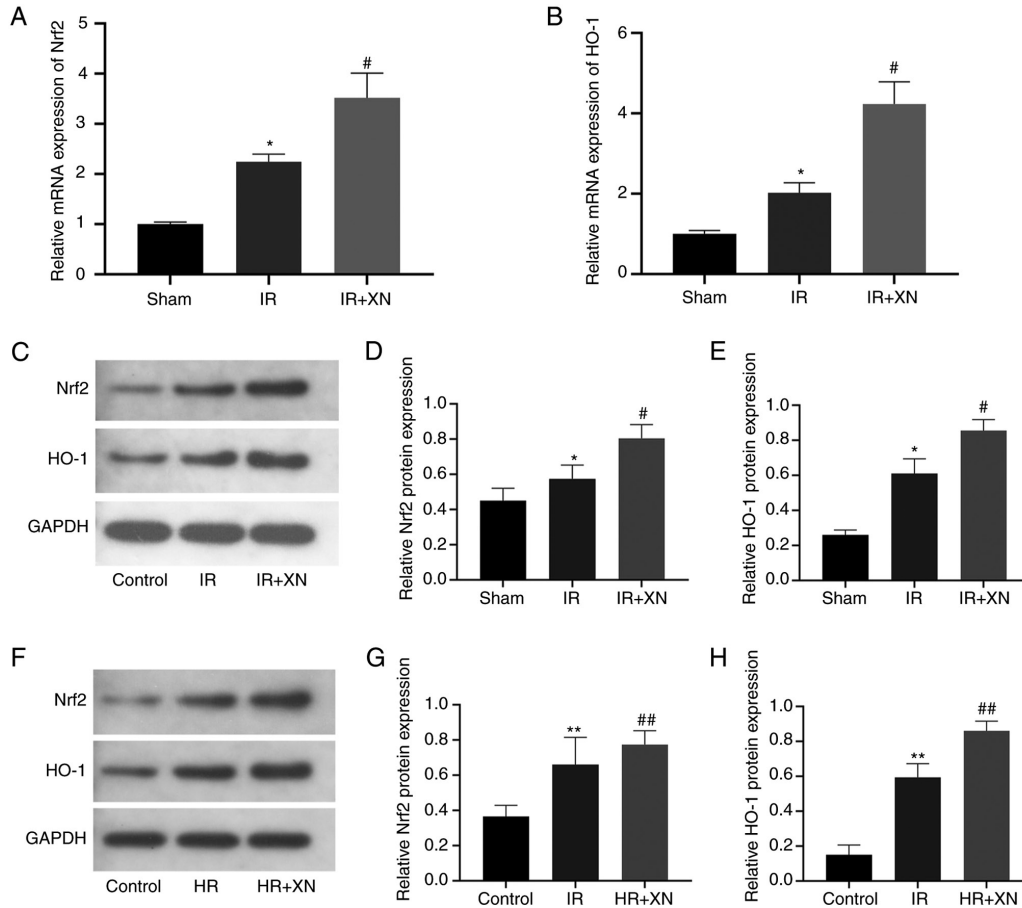


Figure 4. XN upregulates the Nrf2/HO-1 signaling pathway. Reverse transcription-quantitative PCR of (A) Nrf2 and (B) HO-1 mRNA levels in kidney tissues. (C) Western blotting of the proteins (D) Nrf2 and (E) HO-1 in kidney tissues. (F) Western blotting of the proteins (G) Nrf2 and (H) HO-1 in HK-2 cells. * $P < 0.05$ vs. sham, # $P < 0.05$ vs. IR, ** $P < 0.05$ vs. control and ## $P < 0.05$ vs. HR group. XN, xanthohumol; IR, ischemia/reperfusion; HO, heme oxygenase; HR, hypoxia-reoxygenation.

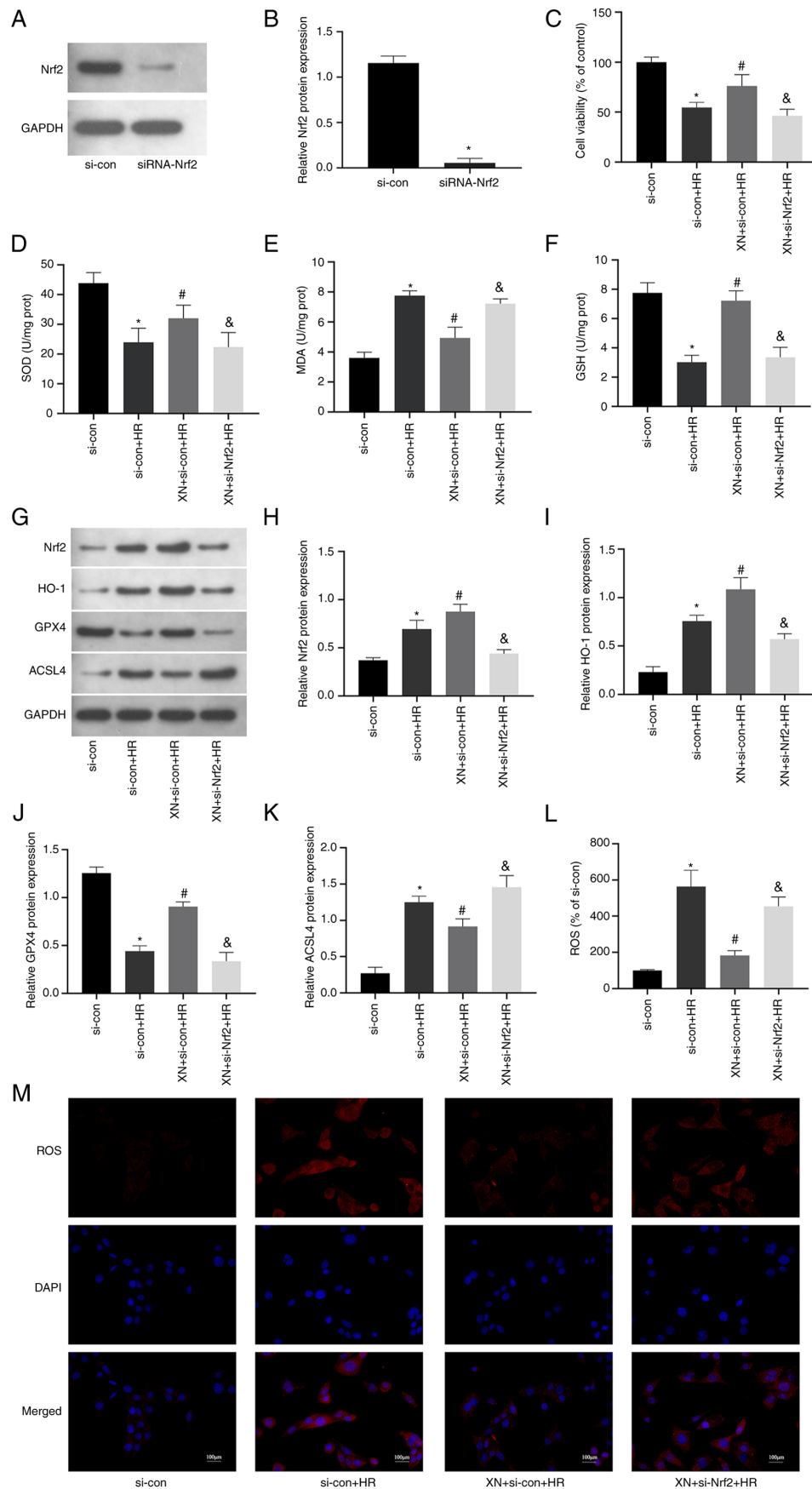


Figure 5. XN inhibits HR-induced ferroptosis via the Nrf2/HO-1 pathway. (A) HK-2 cells were transfected with si-Nrf2 or si-con before HR and XN; western blotting was used to examine Nrf2 in cells. (B) Quantitative analysis of Nrf2 expression. (C) Cell Counting Kit-8 was used to evaluate cell viability. (D) SOD, (E) MDA and (F) GSH levels in HK-2 cells. (G) Western blotting of (H) Nrf2, (I) HO-1, (J) GPX4 and (K) ACSL4 in HK-2 cells. (L and M) ROS production in HK-2 cells was measured by the 2,7-dichlorofluorescein diacetate fluorescent probe; magnification, x400. * $P < 0.05$ vs. si-con, # $P < 0.05$ vs. si-con + HR, & $P < 0.05$ vs. XN + si-con + HR. si-con, negative control small interfering RNA; XN, xanthohumol; ROS, reactive oxygen species; HR, hypoxia-reoxygenation; SOD, superoxide dismutase; prot, protein; MDA, malondialdehyde; GSH, glutathione; GPX4, glutathione peroxidase 4; ACSL4, long-chain acyl-CoA synthetase.

of tumor-associated vascular growth factors, such as vascular endothelial growth factor and interleukin-8 (40). While previous studies have indicated the protective effects of XN on organs, including the liver (41), heart (19) and cranial nerves (42), its renal protective effects have not been fully explored. The present study found that XN protects renal function after IRI and decreases the injury of renal tubular epithelial cells; to the best of our knowledge, the present study is the first to demonstrate the renal protective effect of XN in rats.

Ferroptosis was previously identified as a form of cell death (10). Studies have reported ferroptosis in certain animal models of IRI in vital organs and the level of cell death indicates the degree of IRI (43-45). Numerous studies have shown that ferroptosis is associated with the pathophysiological mechanism of RIRI (46-48), which is essential for exploring disease pathogenesis and discovering novel therapeutic targets. The present study showed that XN inhibited oxidative stress levels in rats with RIRI and expression of ACSL4, but increased the expression of GPX4 during IR. These results suggested that XN was involved in the ferroptosis process of renal cells and decreased RIRI by inhibiting ferroptosis in renal cells. Additionally, the Nrf2/HO-1 signaling pathway serves a notable role in anti-oxidative stress activation in cells (49-51). When IRI occurs, oxidative stress increases and ferroptosis occurs in renal tubular epithelial cells. At the same time, the antioxidant system is activated, thus activating the Nrf2/HO-1 signaling pathway to exert its organ protective effect (52,53), inhibiting oxidative stress and ferroptosis. The present study showed that XN activated the Nrf2/HO-1 signaling pathway in the presence of RIRI and blocking of the Nrf2/HO-1 signaling pathway significantly inhibited the resistance to ferroptosis induced by XN. Therefore, XN exerted anti-oxidative stress and anti-ferroptosis effects by activating the Nrf2/HO-1 pathway.

In conclusion, XN decreased RIRI and improved renal function in rats, and its mechanism may involve activation of the Nrf2/HO-1 signaling pathway to inhibit ferroptosis in renal cells. However, the current study has limitations. The effect of blocking the Nrf2/HO-1 signaling pathway on inhibition of ferroptosis by XN was only explored *in vitro* and animal experiments should be conducted in future studies.

Acknowledgements

Not applicable.

Funding

The present study was supported by Science and Technology Major Project of Hubei Province (grant no. 2019AEA170).

Availability of data and materials

The datasets used and/or analyzed during the current study are available from the corresponding author on reasonable request.

Authors' contributions

ZT designed and carried out the experiments and wrote the manuscript. YF carried out part of the experiment and completed data collection and analysis. WN carried out part

of the experiment and analyzed data. CL assisted in designing the experiment and writing the manuscript. All authors have confirmed the authenticity of all the raw data and have read and approved the final manuscript.

Ethics approval and consent to participate

The present study was conducted in accordance with the Helsinki Declaration II and approved by the Institutional Review Boards of Renmin Hospital of Wuhan University (approval no. K2021-06-023).

Patient consent for publication

Not applicable.

Competing interests

The authors declare that they have no competing interests.

References

1. Tang J and Zhuang S: Histone acetylation and DNA methylation in ischemia/reperfusion injury. *Clin Sci* 133: 597-609, 2019.
2. Wu M, Yiang G, Liao W, Tsai AP, Cheng YL, Cheng PW, Li CY and Li CJ: Current mechanistic concepts in ischemia and reperfusion injury. *Cell Physiol Biochem* 46: 1650-1667, 2018.
3. Cadenas S: ROS and redox signaling in myocardial ischemia-reperfusion injury and cardioprotection. *Free Radical Biol Med* 117: 76-89, 2018.
4. Ampofo E, Berg JJ, Menger MD and Laschke MW: Maslinic acid alleviates ischemia/reperfusion-induced inflammation by downregulation of NFkappaB-mediated adhesion molecule expression. *Sci Rep* 9: 6119, 2019.
5. Tuo QZ, Lei P, Jackman KA, Li XL, Xiong H, Li XL, Liuyang ZY, Roisman L, Zhang ST, Ayton S, *et al*: Tau-mediated iron export prevents ferroptotic damage after ischemic stroke. *Mol Psychiatry* 22: 1520-1530, 2017.
6. Jiang GP, Liao YJ, Huang LL, Zeng XJ and Liao XH: Effects and molecular mechanism of pachymic acid on ferroptosis in renal ischemia reperfusion injury. *Mol Med Rep* 23: 63, 2021.
7. Liu XB and Liu WJ: The role of regulated cell death in renal ischemia-reperfusion injury. *Sheng Li Xue Bao* 74: 320-332, 2022 (In Chinese).
8. Cui X, Lin L, Sun X, Wang L and Shen R: Curcumin protects against renal ischemia/reperfusion injury by regulating oxidative stress and inflammatory response. *Evid Based Complement Alternat Med* 2021: 8490772, 2021.
9. Latunde-Dada GO: Ferroptosis: Role of lipid peroxidation, iron and ferritinophagy. *Biochim Biophys Acta Gen Subj* 1861: 1893-1900, 2017.
10. Dixon SJ, Lemberg KM, Lamprecht MR, Skouta R, Zaitsev EM, Gleason CE, Patel DN, Bauer AJ, Cantley AM, Yang WS, *et al*: Ferroptosis: An iron-dependent form of nonapoptotic cell death. *Cell* 149: 1060-1072, 2012.
11. Linkermann A, Skouta R, Himmerkus N, Mulay SR, Dewitz C, De Zen F, Prokai A, Zuchtriegel G, Krombach F, Welz PS, *et al*: Synchronized renal tubular cell death involves ferroptosis. *Proc Natl Acad Sci USA* 111: 16836-16841, 2014.
12. Tao W, Liu F, Zhang J, Fu S, Zhan H and Qian K: miR-3587 inhibitor attenuates ferroptosis following renal ischemia-reperfusion through HO-1. *Front Mol Biosci* 8: 789927, 2021.
13. Wang J, Chen JJ, Huang JH, Lv BD, Huang XJ, Hu Q, Fu J, Huang WJ and Tao TT: Protective effects of total flavonoids from *Lysimachia christinae* on calcium oxalate-induced oxidative stress in a renal cell line and renal tissue. *Evid Based Complement Alternat Med* 2021: 6667902, 2021.
14. Peluso MR, Miranda CL, Hobbs DJ, Proteau RR and Stevens JF: Xanthohumol and related prenylated flavonoids inhibit inflammatory cytokine production in LPS-activated THP-1 monocytes: structure-activity relationships and *in silico* binding to myeloid differentiation protein-2 (MD-2). *Planta Med* 76: 1536-1543, 2010.

15. Liu M, Hansen PE, Wang G, Qiu L, Dong J, Yin H, Qian Z, Yang M and Miao J: Pharmacological profile of xanthohumol, a prenylated flavonoid from hops (*Humulus lupulus*). *Molecules* 20: 754-779, 2015.
16. Yen TL, Hsu CK, Lu WJ, Hsieh CY, Hsiao G, Chou DS, Wu GJ and Sheu JR: Neuroprotective effects of xanthohumol, a prenylated flavonoid from hops (*Humulus lupulus*), in ischemic stroke of rats. *J Agric Food Chem* 60: 1937-1944, 2012.
17. Oberbauer E, Urmann C, Steffenhagen C, Bieler L, Brunner D, Furtner T, Humpel C, Bäumer B, Bandtlow C, Couillard-Despres S, *et al*: Chroman-like cyclic prenylflavonoids promote neuronal differentiation and neurite outgrowth and are neuroprotective. *J Nutr Biochem* 24: 1953-1962, 2013.
18. Huo H, Zhou Z, Qin J, Liu W, Wang B and Gu Y: Erastin disrupts mitochondrial permeability transition pore (mPTP) and induces apoptotic death of colorectal cancer cells. *PLoS One* 11: e0154605, 2016.
19. Lin JH, Yang KT, Lee WS, Ting PC, Luo YP, Lin DJ, Wang YS and Chang JC: Xanthohumol protects the rat myocardium against ischemia/reperfusion injury-induced ferroptosis. *Oxid Med Cell Longev* 2022: 9523491, 2022.
20. Ma H, Wang X, Zhang W, Li H, Zhao W, Sun J and Yang M: Melatonin suppresses ferroptosis induced by high glucose via activation of the Nrf2/HO-1 signaling pathway in type 2 diabetic osteoporosis. *Oxid Med Cell Longev* 2020: 9067610, 2020.
21. Paller MS: Free radical-mediated posts ischemic injury in renal transplantation. *Ren Fail* 14: 257-260, 1992.
22. Livak KJ and Schmittgen TD: Analysis of relative gene expression data using real-time quantitative PCR and the 2(-Delta Delta C(T)) method. *Methods* 25: 402-408, 2001.
23. Sundaresan M, Yu ZX, Ferrans VJ, Irani K and Finkel T: Requirement for generation of H2O2 for platelet-derived growth factor signal transduction. *Science* 270: 296-299, 1995.
24. Kellum JA, Romagnani P, Ashuntantang G, Ronco C, Zarbock A and Anders HJ: Acute kidney injury. *Nat Rev Dis Primers* 7: 52, 2021.
25. Ronco C, Bellomo R and Kellum JA: Acute kidney injury. *Lancet* 394: 1949-1964, 2019.
26. Martin LC: Naringin, trimetazidine and baroreflex in renal ischemia-reperfusion injury. *Arq Bras Cardiol* 117: 298-299, 2021.
27. Kim K, Yang H, Yi J, Son HE, Ryu JY, Kim YC, Jeong JC, Chin HJ, Na KY, Chae DW, *et al*: Real-time clinical decision support based on recurrent neural networks for in-hospital acute kidney injury: External validation and model interpretation. *J Med Internet Res* 23: e24120, 2021.
28. Paragas N, Qiu A, Zhang Q, Samstein B, Deng SX, Schmidt-Ott KM, Viltard M, Yu W, Forster CS, Gong G, *et al*: The Ngal reporter mouse detects the response of the kidney to injury in real time. *Nat Med* 17: 216-222, 2011.
29. Su X, Zhou M, Li Y, Zhang J, An N, Yang F, Zhang G, Yuan C, Chen H, Wu H and Xing Y: Protective effects of natural products against myocardial ischemia/reperfusion: Mitochondria-targeted therapeutics. *Biomed Pharmacother* 149: 112893, 2022.
30. Li K, Xiao K, Zhu S, Wang Y and Wang W: Chinese herbal medicine for primary liver cancer therapy: Perspectives and challenges. *Front Pharmacol* 13: 889799, 2022.
31. Chen W, Becker T, Qian F and Ring J: Beer and beer compounds: Physiological effects on skin health. *J Eur Acad Dermatol Venereol* 28: 142-150, 2014.
32. Krajnovic T, Kaluderovic GN, Wessjohann LA, Mijatovic S and Maksimovic-Ivanic D: Versatile antitumor potential of isoxanthohumol: Enhancement of paclitaxel activity in vivo. *Pharmacol Res* 105: 62-73, 2016.
33. Negrao R, Costa R, Duarte D, Taveira GT, Mendanha M, Moura L, Vasques L, Azevedo I and Soares R: Angiogenesis and inflammation signaling are targets of beer polyphenols on vascular cells. *J Cell Biochem* 111: 1270-1279, 2010.
34. Negrao R, Duarte D, Costa R and Soares R: Isoxanthohumol modulates angiogenesis and inflammation via vascular endothelial growth factor receptor, tumor necrosis factor alpha and nuclear factor kappa B pathways. *Biofactors* 39: 608-622, 2013.
35. Cho YC, You SK, Kim HJ, Cho CW, Lee IS and Kang BY: Xanthohumol inhibits IL-12 production and reduces chronic allergic contact dermatitis. *Int Immunopharmacol* 10: 556-561, 2010.
36. Kiyofuji A, Yui K, Takahashi K and Osada K: Effects of xanthohumol-rich hop extract on the differentiation of preadipocytes. *J Oleo Sci* 63: 593-597, 2014.
37. Izzo G, Soder O and Svechnikov K: The prenylflavonoid phytoestrogens 8-prenylnaringenin and isoxanthohumol differentially suppress steroidogenesis in rat Leydig cells in ontogenesis. *J Appl Toxicol* 31: 589-594, 2011.
38. Dorn C, Kraus B, Motyl M, Weiss TS, Gehrig M, Scholmerich J, Heilmann J and Hellerbrand C: Xanthohumol, a chalcon derived from hops, inhibits hepatic inflammation and fibrosis. *Mol Nutr Food Res* 54 (Suppl 2): S205-S213, 2010.
39. Albini A, Dell'Eva R, Vene R, Ferrari N, Buhler DR, Noonan DM and Fassina G: Mechanisms of the antiangiogenic activity by the hop flavonoid xanthohumol: NF-kappaB and Akt as targets. *FASEB J* 20: 527-529, 2006.
40. Saito K, Matsuo Y, Imafuji H, Okubo T, Maeda Y, Sato T, Shamoto T, Tsuboi K, Morimoto M, Takahashi H, *et al*: Xanthohumol inhibits angiogenesis by suppressing nuclear factor- κ B activation in pancreatic cancer. *Cancer Sci* 109: 132-140, 2018.
41. Dorn C, Massinger S, Wuzik A, Heilmann J and Hellerbrand C: Xanthohumol suppresses inflammatory response to warm ischemia-reperfusion induced liver injury. *Exp Mol Pathol* 94: 10-16, 2013.
42. Jiao Y, Cao Y, Lu X, Wang J, Saitgareeva A, Kong X, Song C, Li J, Tian K, Zhang S, *et al*: Xanthohumol protects neuron from cerebral ischemia injury in experimental stroke. *Mol Biol Rep* 47: 2417-2425, 2020.
43. Friedmann AJP, Schneider M, Proneth B, Tyurina YY, Tyurin VA, Hammond VJ, Herbach N, Aichler M, Walch A, Eggenhofer E, *et al*: Inactivation of the ferroptosis regulator Gpx4 triggers acute renal failure in mice. *Nat Cell Biol* 16: 1180-1191, 2014.
44. Gao M, Monian P, Quadri N, Ramasamy R and Jiang X: Glutaminolysis and transferrin regulate ferroptosis. *Mol Cell* 59: 298-308, 2015.
45. Gascon S, Murenu E, Masserdotti G, Ortega F, Russo GL, Petrik D, Deshpande A, Heinrich C, Karow M, Robertson SP, *et al*: Identification and successful negotiation of a metabolic checkpoint in direct neuronal reprogramming. *Cell Stem Cell* 18: 396-409, 2016.
46. Pan J, Zhao J, Feng L, Xu X, He Z and Liang W: Inhibition of USP14 suppresses ROS-dependent ferroptosis and alleviates renal ischemia/reperfusion injury. *Cell Biochem Biophys* 81: 87-96, 2023.
47. Qi Y, Hu M, Qiu Y, Zhang L, Yan Y, Feng Y, Feng C, Hou X, Wang Z, Zhang D and Zhao J: Mitoglitazone ameliorates renal ischemia/reperfusion injury by inhibiting ferroptosis via targeting mitoNEET. *Toxicol Appl Pharmacol* 465: 116440, 2023.
48. Dong B, Ding C, Xiang H, Zheng J, Li X, Xue W and Li Y: USP7 accelerates FMR1-mediated ferroptosis by facilitating TBK1 ubiquitination and DNMT1 deubiquitination after renal ischemia-reperfusion injury. *Inflamm Res* 71: 1519-1533, 2022.
49. Shen B, Zhao C, Wang Y, Peng Y, Cheng J, Li Z, Wu L, Jin M and Feng H: Aucubin inhibited lipid accumulation and oxidative stress via Nrf2/HO-1 and AMPK signalling pathways. *J Cell Mol Med* 23: 4063-4075, 2019.
50. Di Tu Q, Jin J, Hu X, Ren Y, Zhao L and He Q: Curcumin improves the renal autophagy in rat experimental membranous nephropathy via regulating the PI3K/AKT/mTOR and Nrf2/HO-1 signaling pathways. *Biomed Res Int* 2020: 7069052, 2020.
51. Loboda A, Damulewicz M, Pyza E, Jozkowicz A and Dulak J: Role of Nrf2/HO-1 system in development, oxidative stress response and diseases: An evolutionarily conserved mechanism. *Cell Mol Life Sci* 73: 3221-3247, 2016.
52. Qiao J, Ma H, Chen M and Bai J: Vitamin D alleviates neuronal injury in cerebral ischemia-reperfusion via enhancing the Nrf2/HO-1 antioxidant pathway to counteract NLRP3-mediated pyroptosis. *J Neuropathol Exp Neurol* 82: 722-733, 2023.
53. Li X, Yi L, Liu X, Chen X, Chen S and Cai S: Isoquercitrin played a neuroprotective role in rats after cerebral ischemia/reperfusion through Up-regulating neuroglobin and anti-oxidative stress. *Transplant Proc* 55: 1751-1761, 2023.

